

Stress fluctuations and shear thickening in dense granular suspensionsQin Xu,^{1,2} Abhinendra Singh,^{1,3} and Heinrich M. Jaeger^{1,4}¹⁾*James Franck Institute, University of Chicago, IL, 60637 USA*²⁾*Department of Materials, ETH Zurich, 8093 Zurich, Switzerland*³⁾*Pritzker School of Molecular Engineering, University of Chicago, IL, 60637 USA*⁴⁾*Department of Physics, University of Chicago, IL, 60637 USA*

We experimentally investigate the rheology and stress fluctuations of granules densely suspended in silicone oil. We find that both thickening strength and stress fluctuations significantly weaken with oil viscosity η_0 . Comparison of our rheological results to the Wyart-Cates model for describing different dynamic jamming states suggests a transition from frictional contacts to lubrication interactions as η_0 increases. To clarify the contribution from viscous interactions to the rheology, we systematically measure stress fluctuations in various flow states. Reduction of stress fluctuations with η_0 indicates that a strong lubrication layer greatly inhibits force correlations among particles. Measuring stress fluctuations in the strong shear thickening regime, we observe a crossover from asymmetric Gamma to symmetric Gaussian distributions and associated with it a decrease of lateral (radial) correlation length ξ with increasing shear rate.

I. INTRODUCTION

Concentrated particle suspensions are found in both nature and industry^{1,2}. Dense granular suspensions are mixtures of non-Brownian particles (diameter $\geq 1\mu m$) and viscous liquids at high volume fractions, and can exhibit complex flow behaviors far from Newtonian fluids³⁻⁵. Because of the large solid fraction ϕ , direct contacts between grains are crucial in governing the rheology^{4,6,7}. Similar to dry granular materials, dense granular suspensions can dilate against a boundary under flow⁸. As the dilation is counteracted by confinement, particles are likely to rearrange and create dynamic force networks via frictional contacts. As a critical volume fraction is approached, a steep jump in flow resistance with shear rate can be observed, a phenomenon called discontinuous shear thickening (DST)^{4,7,9-11}. However, viscous interactions can also be significant in suspensions as grains are close to each other at high volume fractions^{12,13}. For instance, the contribution of lubrication forces to shear thickening has been discussed extensively. Depending on the system, viscous coupling has been found to enhance^{14,15}, weaken¹⁶ or not affect shear thickening¹⁷.

Recent studies^{6,7,17-23} have shown that strong shear thickening is a stress-driven transition from a lubricated “frictionless” to an unlubricated “frictional” state. A critical stress τ_c is required to squeeze out the lubrication layer present between the particles and bring them into frictional contacts. This critical stress could originate from the repulsive force due to steric (e.g. due to adsorbed polymer) or electrostatic stabilization as well as Brownian force, since all these forces essentially keep the particles apart as long as the shear stresses are smaller than a certain threshold level. The frictional forces are influenced by particle roughness^{18,24,25} or chemical surface interactions²⁶. The behavior can be thus divided into two regimes that are essentially rate independent, i.e., states in which the stresses are linear with strain rate. One is the low-stress regime ($\tau \ll \tau_c$), where particles interact through lubrication forces, with the rheology diverging at the frictionless jamming point ϕ_J^0 . In this case, the viscosity is affected by the long-ranged attractive or short-ranged repulsive forces^{27,28}. The second regime is at high stresses ($\tau \gg \tau_c$), where almost all particles come into direct, frictional contacts, and the viscosity (and also the normal stresses) diverge at a volume fraction $\phi_J^\mu < \phi_J^0$ that depends on the interparticle friction coefficient μ . With increasing stress τ , the crossover between these two rate independent regimes results in the shear thickening behavior. Thus, a complete description of the dynamics of dense granular

suspensions requires the understanding of both frictional and viscous interactions.

Prior works have indicated that stresses in a dense particulate suspension can exhibit strong fluctuations^{24,29,30}. Here we exploit the fact that the statistical features of globally measured stress fluctuations may help to understand the contributions of different local interactions to the underlying rheology. For dry granular materials, stress fluctuations and their distributions are of importance in identifying the frictional contacts and micro-structures in different mechanical states, such as jamming, yielding, strain stiffening and shear banding^{31–36}. Sheared dense suspensions share the importance of frictional interactions with dry granular media. However, the link between stress fluctuations and time-averaged flow properties, such as the effective suspension viscosity that emerges from the interplay of lubrication and friction has not been investigated systematically in the DST regime.

We show quantitatively that, as the solvent viscosity increases, the lubrication interactions greatly reduce frictional contacts, and we observe significant weakening of both shear thickening and stress fluctuations. Comparing stress distributions for increasing sample sizes, we systematically measure spatial correlations in the strong shear thickening regime. Our results show that stress correlations are also weakened by viscous interactions. The work presented here not only demonstrates a different approach to control thickening but also reveals how local statistical properties, in this case stress fluctuations, are linked to the global rheology of dense granular suspensions.

II. METHODS: EXPERIMENTAL SETUP AND MODEL

A. Experimental setup

Two different hard particle suspensions are studied in our experiments: glass spheres and ZrO₂ beads suspended in silicone oil. Glass beads (average diameter $22 \pm 5 \mu\text{m}$) disperse well in silicone oil and are chosen as a typical shear thickener with low yield stress. For imaging the boundary profile at the free surface of the suspension we use ZrO₂ particles that are larger ($200 \pm 10 \mu\text{m}$ in diameter) and less reflective than glass. To adjust the viscous interactions in the suspensions, the viscosity (η_0) of the silicone oil is varied from 20 cSt to 1.8×10^4 cSt by tuning the molecular weight of the polymer chains from 10^3 to 10^6

g/mole. For this range of solvent viscosities, particle inertia can be neglected.

Flow properties are measured with an Anton Paar PCR301 rheometer using a parallel-plate geometry. Care is taken to make sure no fluid extended outside the parallel plates so the grains are confined to the space between the plates by liquid surface tension. For rheological measurements of steady state flow, we shear suspensions by gradually ramping up shear rate $\dot{\gamma}$. For each $\dot{\gamma}$, we measure shear stress τ and viscosity is calculated by the ratio $\tau/\dot{\gamma}$. For measurements of stress fluctuations, we keep shear rate $\dot{\gamma}$ unchanged and measure shear stress evolving with time, $\tau(t)$.

B. Model

Below, we summarize the current phenomenological approach to model the rheology of dense suspensions. The basic assumption^{9,21,37} is that the relative viscosity $\eta_r = \eta(\phi, \tau)/\eta_0$ is in distinct stress-independent states both at low and high stresses. The viscosity η_r is thus simply a function of the packing fraction ϕ at low ($\tau \ll \tau_c$) and high ($\tau \gg \tau_c$) stress states and can be expressed as

$$\eta_r^L(\phi) = (1 - \phi/\phi_J^0)^{-2} \quad (1a)$$

$$\eta_r^H(\phi, \mu) = (1 - \phi/\phi_J^\mu)^{-2}, \quad (1b)$$

where ϕ_J^0 and ϕ_J^μ denote the jamming volume fractions for $\mu = 0$ (lubricated, frictionless state) and nonzero values of μ (frictional state), respectively.

Next, to introduce the stress dependence on viscosity and to capture the transition between the lubrication dominated and frictionally dominated states, a stress-dependent jamming volume fraction is specified using an expression similar to that proposed by Wyart and Cates⁹

$$\phi_m(\tau) = \phi_J^\mu f(\tau) + \phi_J^0 [1 - f(\tau)], \quad (2)$$

where $f(\tau)$ denotes the fraction of particle interactions for which the shear force exceeds the critical force F_c to bring the particles into direct frictional contact. Using (1), and (2) the stress dependent viscosity $\eta_r(\phi, \tau)$ can be expressed as:

$$\eta_r(\phi, \tau) = [1 - \phi/\phi_m(\tau)]^{-2}. \quad (3)$$

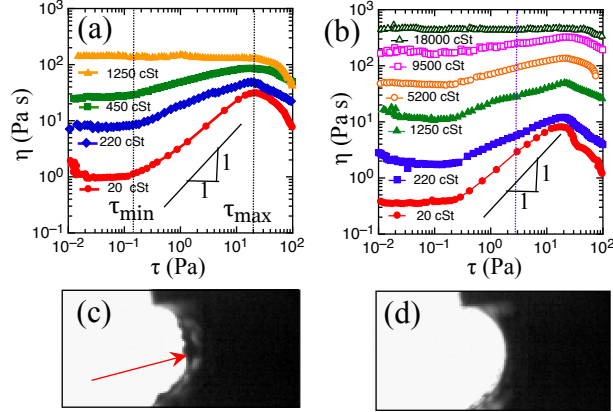


FIG. 1. **Rheology.** Flow curves of suspension viscosity (η) vs. stress (τ) for (a) $22\mu\text{m}$ glass beads in oil with volume fraction $\phi = 55\%$ and (b) $203\mu\text{m}$ ZrO_2 particles in oil with volume fraction $\phi = 56\%$ for different oil viscosities. (c) and (d) are images taken from suspensions containing 20 cSt and 9.5×10^3 cSt silicone oil under a given shear stress $\tau = 2.8$ Pa, respectively. Red arrow: roughness of the interface caused by frustrated dilation.

Before we discuss our results it is important to mention that the experiments performed here are for particles sufficiently dense that they cannot be matched in specific density with the suspending liquid and will settle under gravity. The onset stress for strong shear thickening is therefore not controlled by overcoming electrostatic repulsive forces, as in many colloidal systems. Instead, the minimum stress to bring particles into direct contact is associated with entraining them into the shear flow. This leads to the following picture. The particles are first dispersed within the rheometer and sediment in the absence of any applied shear. As shear is applied, the suspension overcomes the gravitational force, it fluidizes and exhibits thinning behavior as was probed in detail in our previous study¹⁶. In the fluidized state, the suspension now behaves like a density matched non-Brownian (or Brownian) suspension at low stress wherein the lubricated interaction between particles essentially lead to divergence of viscosity at ϕ_j^0 . As the shear rate is ramped up, the contact stresses are able to break the lubrication layer between particles and interparticle friction then leads to shear thickening as observed in other dense suspensions^{4,5}.

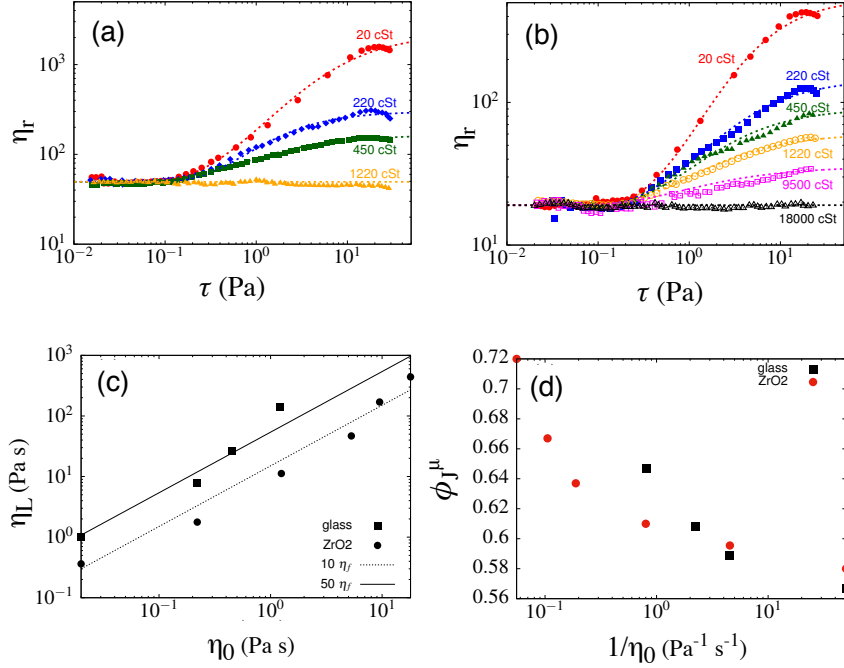


FIG. 2. **Rheological analysis.** Relative viscosity η_r as a function of stress τ for (a) glass-oil (for $\phi = 55\%$) and (b) ZrO_2 -oil (for $\phi = 56\%$) suspensions. Symbols are experimental data with different solvent viscosity η_0 as indicated with lines that represent a fit to Eq. (3). (c) Viscosity of the low stress (lubricated) state plotted as a function of the solvent viscosity η_0 . (d) Frictional jamming volume fraction ϕ_j^μ plotted as a function of inverse solvent viscosity $1/\eta_0$ for glass-oil and ZrO_2 -oil suspensions.

III. RESULTS

A. Rheological analysis

Figure 1(a) shows flow curves for dense glass-oil suspensions in varying viscosities of silicone oil for a constant volume fraction $\phi = 55\%$. For $\eta_0 = 20, 220, 450$ cSt, shear thickening is observed within the same stress range between τ_{min} and τ_{max} . The onset stress $\tau_{min} \approx 0.14$ Pa indicates the minimum stress required to rearrange the particle configurations by overriding the gravity⁸, and the ending stress $\tau_{max} \approx 20$ Pa is set by the maximum Laplace pressure acting on the particles at the suspension-air interface without moving the contact line¹⁶. Given the fact that both τ_{min} and τ_{max} are independent of solvent viscosity, the two

bounds of shear thickening are not varied by the viscous dissipation in the suspensions. The degree of the shear thickening, however, changes dramatically with η_0 .

Taking the suspension with $\eta_0 = 20$ cSt (red solid circles in Fig.1(a)) as an example, we observe an approximate $\eta \sim \tau$ relation, which indicates an abrupt, almost continuous increase of viscosity at a critical shear rate $\dot{\gamma}_c$. The value of $\dot{\gamma}_c$ for the viscosity jump is given by the slope of $\eta(\tau)$. As we increase η_0 , we observe a crossover from strong shear thickening to stress independent flow behavior. As shown in Fig. 1a, shear thickening weakens for 220 cSt (blue diamonds) and 450 cSt (green squares), and vanishes at $\eta_0 = 1250$ cSt (orange triangles). A similar crossover is also observed for ZrO₂-oil suspensions (Fig. 1(b)). In this case, a much larger oil viscosity ($\eta_0 \approx 1.8 \times 10^4$ cSt) is required to obscure shear thickening and achieve a rate independent behavior. In such a highly viscous limit, each stress data point is taken by averaging 10^4 results over a period of 2 hours to ensure steady state.

We image the interface of ZrO₂ suspensions *in-situ* as rheological measurements are performed. The suspensions are lit from behind as a camera focuses on the interface. The profile is highlighted by the contrast between white background and dark suspensions. As shown in Figs. 1(c)&(d), we compare the surface profiles between $\eta_0 = 20$ cSt (Fig. 1c) and $\eta_0 = 9.5 \times 10^3$ cSt (Fig. 1d) under a same shear stress $\tau = 2.8$ Pa in shear thickening regime. For $\eta_0 = 20$ cSt, interface is roughened by the protruded particles as shear thickening occurs, which is consistent with frustrated dilation⁸. For $\eta_0 = 9.5 \times 10^3$ cSt, however, the suspension interface remains smooth and liquid-like.

At low stresses ($\tau < \tau_{min}$), since the lubrication film is present between the particles, the viscosity of suspension η_L is expected to scale with the solvent viscosity η_0 . The low stress viscosity η_L for both glass-oil and ZrO₂-oil suspensions is displayed as a function of η_0 in Fig. 2c, and we recover a linear relation between the them as $\eta \propto \eta_0$. Some of the deviations from the linear trend could arise from the existence of a yield stress or could be associated with the difficulty of mixing of solid particles homogeneously in highly viscous fluid at high volume fractions $\phi \sim 0.55$. Figures 2a and b display the relative viscosity η_r as a function of stress τ for glass-oil and ZrO₂-oil suspensions for various values of solvent viscosity η_0 . In these plots we have used the relations displayed in Fig. 2c to extract the relative viscosity η_r , to collapse the viscosity data at low stresses. We observe that the high-stress frictional viscosity η_H decreases with increase in the solvent viscosity, and also the extent of shear thickening decreases with increase in solvent viscosity η_0 . The decrease in η_H suggests that

higher molecular weight makes it difficult to bring the particles into direct, frictional contact.

Simulations have demonstrated that, for a given volume fraction, the viscosity of the frictional state and hence the extent of thickening decreases with the decrease in interparticle friction coefficient μ ^{19,37}, while the onset stress for shear thickening is independent of μ . The flow–curves reported in Figs. 2a and b for different η_0 clearly show a very similar behavior. To test the hypothesis that direct frictional contacts and hence contact force networks drive the observed changes with different molecular weight solvent, the friction–based model of Refs.^{9,37} is fit to the shear–thickening portion ($\tau_{\min} < \tau < \tau_{\max}$) of all viscosity curves. As the last missing ingredient in Eq. (3), the fraction of particles in direct, frictional contacts $f(\tau)$ is expressed as a $f(\tau) = \exp(-\tau^*/\tau)$, where τ^* is the critical stress for particles to overcome the critical force.

The friction-based model (Eq. (3)) very well describes the shear thickening in samples with variable η_0 (Fig. 2a,b) using fixed ϕ_J^0 and τ^* and variable ϕ_J^μ for glass bead and ZrO₂ suspensions. The resulting parameters $\phi_J^0 = 0.65$ and $\tau^* = 0.45$ for glass–oil, and $\phi_J^0 = 0.72$ and $\tau^* = 0.55$ for ZrO₂–oil suspensions were found to be independent of η_0 . Previous work for hard–sphere colloidal suspensions reported a value of $\phi_J^0 = 0.71$ ³⁸.

Since τ^* is found to be independent of the solvent viscosities η_0 , this indicates that polymers with different molecular weight do not affect the critical force needed to bring particles into frictional contact. Whereas ϕ_J^0 and τ^* are found to be insensitive to η_0 , the striking result here is that the frictional jamming point ϕ_J^μ shows a pronounced increase with η_0 . This increase in ϕ_J^μ is consistent with the thought that an increase in polymer molecular weight inhibits the formation of frictional contacts and the development of a system–spanning frictional contact network.

B. Stress fluctuations

To further validate our hypothesis that weakening of frictional contacts with increasing η_0 drives the observed change in rheology, we now turn our attention to the stress fluctuations. Previous studies^{29,39,40} have shown that dense hard–sphere suspensions can exhibit pronounced fluctuations and that the magnitude of these fluctuations depends on the closeness to the DST transition. However none of these studies have related the fluctuations to interparticle forces.

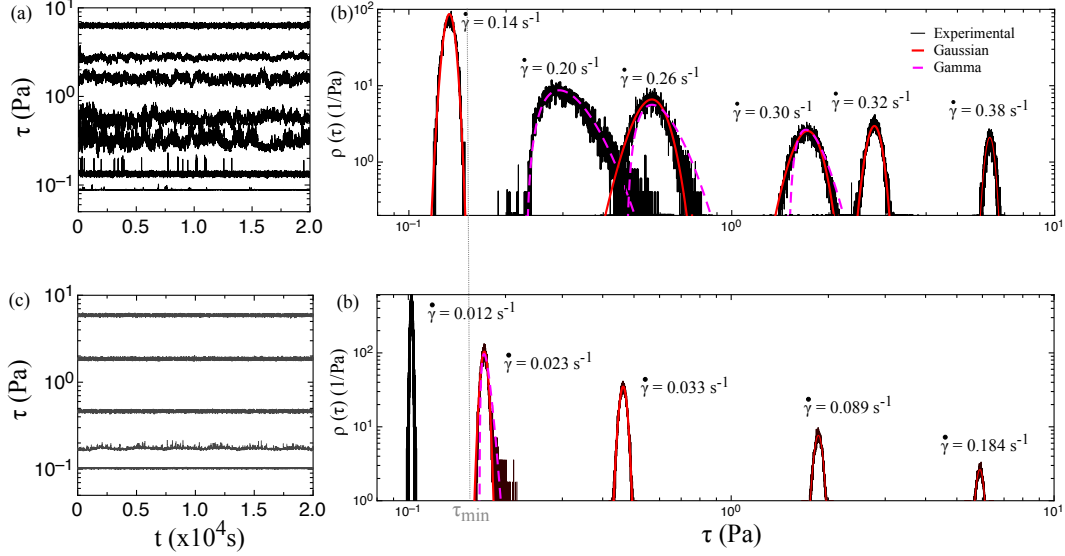


FIG. 3. **Shear stress fluctuations.** (a) Time evolution of stress for shear rates at $\dot{\gamma} = 0.09, 0.14, 0.20, 0.26, 0.30, 0.32, 0.38 \text{ s}^{-1}$ (from the bottom to top), measured for glass beads in 20 cSt silicone oil. (b) Probability density distribution functions $\rho(\tau)$ as from the fluctuation data in (a) for $\dot{\gamma} = 0.14, 0.20, 0.26, 0.30, 0.32, 0.38 \text{ s}^{-1}$. Solid black lines are the experimental results. Red solid lines and pink dashed lines are fits to Gaussian and Gamma distributions. The grey dashed line points at the onset of shear thickening (τ_{min}). Similarly, panel (c) shows the time evolution of stress for shear rates at $\dot{\gamma} = 0.012, 0.023, 0.033, 0.089, 0.184 \text{ s}^{-1}$ (from the bottom to top) for glass beads in 220 cSt silicone oil, and the corresponding distributions are shown in panel (d).

We apply constant shear to glass-oil suspensions to measure the temporal fluctuations of the shear stress $\tau(t)$. In this section, we focus on the comparison of results with $\eta_0 = 20$ and 220 cSt. For the higher solvent viscosity, stress fluctuations are hardly visible. Figure 3(a), for instance, displays the plots of $\tau(t)$ for $\eta_0 = 20$ cSt over a period of 2×10^4 seconds. From bottom to top, each trace corresponds to a different applied shear rate as indicated. When $\dot{\gamma} \geq 0.20 \text{ s}^{-1}$, shear stresses are in the range of shear thickening, $\tau_{min} < \tau(t, \dot{\gamma}) < \tau_{max}$. For the top six traces of $\tau(t, \dot{\gamma})$ in panel (a), we plot the probability density function, $\rho(\tau)$, in panel (b).

The profiles of $\rho(\tau)$ evolve with applied shear rate and shear stress. For $\dot{\gamma} = 0.14 \text{ s}^{-1}$, the corresponding shear stress $\tau|_{\dot{\gamma}=0.14 \text{ s}^{-1}}$ is below shear thickening onset τ_{min} . As a result, we find that $\rho(\tau)$ is well approximated by a Gaussian distribution with a standard deviation set

by the stress resolution of our instruments (~ 0.01 Pa). As soon as the shear stress passes τ_{min} , the fluctuations of shear stress grow significantly and the distribution starts to deviate from Gaussian. At $\dot{\gamma} = 0.20$ s $^{-1}$, for example, the shear stress is only slightly above τ_{min} but $\rho(\tau)$ is no longer symmetric. Instead, $\rho(\tau)$ can be fitted well by a second-order Gamma function

$$\rho(\tau) = \frac{(\tau - \tau_0)^2}{2\tau_1^3} \exp\left(-\frac{(\tau - \tau_0)}{\tau_1}\right), \quad (4)$$

where τ_0 ($\approx 0.23 \pm 0.03$) Pa and τ_1 ($\approx 0.031 \pm 0.008$) Pa are fitting parameters that characterize the mean and the effective width, respectively. Equation (4) is consistent with the results of the so-called q-model, which predicts stress fluctuations from a force chain network connected through direct contacts⁴¹. Such distribution is also found for the normal stress of sheared dry granular media³¹ where frictional interactions dominate particle contacts. However, the distribution becomes less asymmetric as we increase the shear rate, $\dot{\gamma} = 0.26, 0.30, 0.32, 0.38$ s $^{-1}$, driving the shape of $\rho(\tau)$ back to Gaussian again, but with a larger standard deviation ($\sim 10^0$ Pa). Note that the rheometer shear stress noise is significantly smaller ($\sim 10^{-2}$ Pa).

Fluctuations of shear stress greatly reduce for higher oil viscosity. Figures 2c and d show the plots of $\tau(t)$ and $\rho(t)$ for $\eta_0 = 220$ cSt. Clearly, the magnitude of fluctuations decreases significantly. Except possibly for $\dot{\gamma} = 0.023$ s $^{-1}$, $\rho(\tau)$ can be well fitted by Gaussian distributions for most of shear rates and measuring radii. So, why do we see different stress distributions for different flow states in shear thickening regime?

One likely scenario is connected to the stress-dependent contact forces. For $\tau < \tau_{min}$ all contacts are lubricated and the distribution is Gaussian simply due to experimental measurement uncertainty. In the beginning shear thickening ($\tau \sim \tau_{min}$), frictional force chains start to emerge and span to gap between. As shear rate increases in shear thickening regime, more force chains are lined up between plates. It is important to note that Eq.(4) is based on an ensemble average over individually normalized distributions in a static packing of particles. In the steady-state shear experiments, however, the force networks are constantly evolving. Therefore, if the measurement window becomes longer than the reconfiguration time, and if subsequent realizations of the contact force network are uncorrelated, the experiments will record averages over distributions as in Eq.(4). This will lead to a Gaussian-like distribution due to the Central Limit Theorem (CLT), in line with what we observe in Fig.3. When more independent force chains are built up as we are ramping up $\dot{\gamma}$, $\rho(\tau)$ becomes more close to

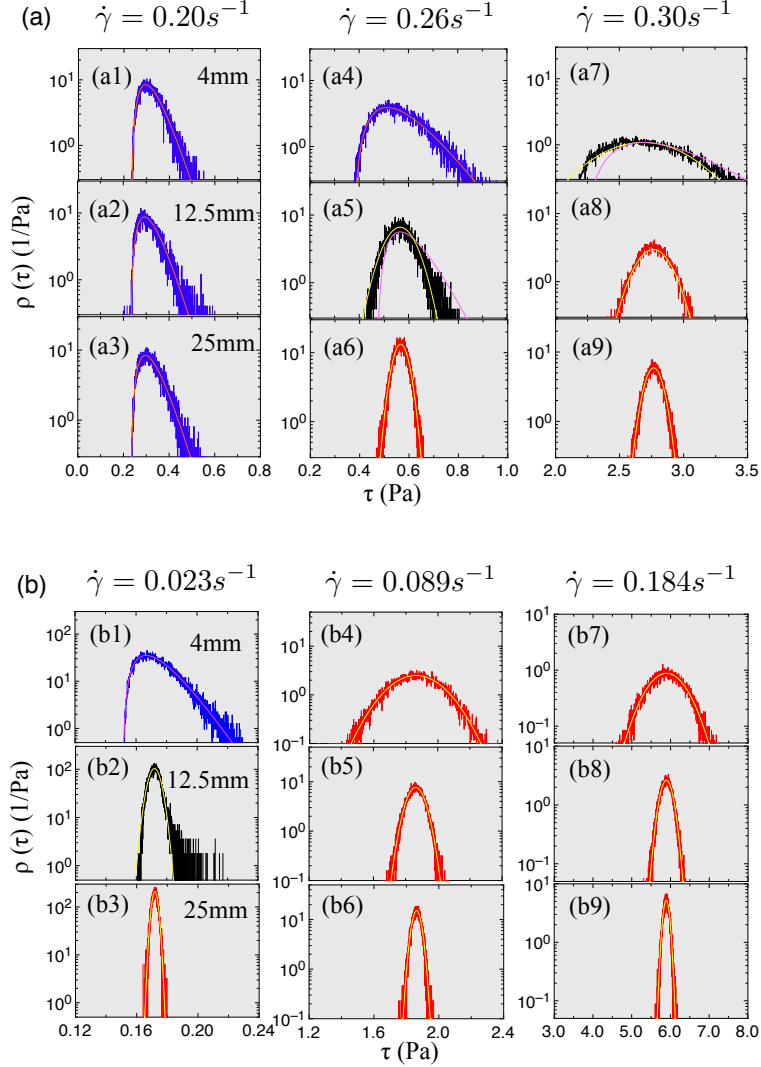


FIG. 4. **System size dependence.** Plots of $\rho(\tau)$ for (a) $\eta_0 = 20$ cSt at different shear rates (columns, left to right: $0.20s^{-1}$, $0.26s^{-1}$ and $0.30s^{-1}$) and (b) $\eta_0 = 220$ cSt at different shear rates (columns, left to right: $0.023s^{-1}$, $0.089s^{-1}$, and $0.184s^{-1}$). From top to bottom: plate size $R_s = 4, 12.5$ and 25 mm.

a Gaussian distribution.

We can further test this scenario by exploring spatial correlations. We do that by measuring the shear stress fluctuations in samples that have a different lateral (radial) extent, which we prepare by varying the volume of suspension placed between plates of a given, fixed spacing. If the sample subdivides into several uncorrelated regions we would expect a reduction in the standard deviation of fluctuations around their mean. Figure 4 shows

the stress fluctuation probability density $\rho(\tau)$ for different sample radii R for both low (a) and high (b) solvent viscosity. Each column shows a different average shear stress, corresponding to $\dot{\gamma} = 0.20, 0.26$ and 0.30 s (left to right). In these panels, we use various colors to indicate different distributions. Blue and red curves are used to present $\rho(\tau)$ that can be fitted well by Gamma and Gaussian distributions, respectively. For $\rho(\tau)$ partly fitted by either Gamma or Gaussian functions, we use black.

In Fig. 4(a), we observe a crossover from Gamma to Gaussian distributions with increasing R . Meanwhile, the standard deviation of $\rho(\tau)$ decreases. The results are indeed similar to the averaging effects in the case of ramping up $\dot{\gamma}$. At low shear rate $\dot{\gamma} = 0.20$ s⁻¹ however, $\rho(\tau)$ is independent of R . The distribution plots in Fig. 4(a1) - (a3) can be nicely fitted with a single set of parameters $\tau_0 = 0.23 \pm 0.05$ Pa and $\tau_1 = 0.031 \pm 0.009$ Pa as R increases from 4 to 25 mm. Therefore, at low stresses in the early stage of shear thickening, all force chains are highly correlated across the whole sample.

As solvent viscosity increases to $\eta_0 = 220$ cSt in Fig. 4b, most of the distribution functions in the panel are nicely fitted by Gaussian distributions (the fitted results are plotted in yellow lines). The only asymmetric Gamma distribution is found at low shear rate $\dot{\gamma} = 0.023$ s⁻¹ with small sample radius $R = 4$ mm. As long as R or $\dot{\gamma}$ increases, $\rho(\tau)$ is quickly averaged into a Gaussian distribution. In contrast to the low-viscosity case, now the standard deviation greatly depends on sample radius. As R increases from 4 to 25 mm, the contact area between the suspension and the plates increases by a factor around 40. According to the CLT, averaging results of independent variables will reduce the standard deviation by a factor of $\sqrt{40} \approx 6.3$, which is consistent with the plots of $\rho(\tau)$ (for example comparing Fig. 4(b4) to (b6)). The results implies that viscous interactions in suspensions weaken stress correlations among particles.

We can make this quantitative by defining a spatial correlation length ξ along the lateral (i.e.e, radial) direction by looking into the change of standard deviation with R . This standard deviation of the fluctuation distributions is defined as $\sigma = \sqrt{(\tau(t) - \tau_{average})^2}$. For a Gaussian distribution the mean stress $\tau_{average}$ and σ follow the usual definitions, while for the Gamma distribution in Eq.(4) $\tau_{average} = \tau_0 + 3\tau_1$ and $\sigma = \sqrt{3}\tau_1$. When $R \gg \xi$, the suspension includes N sub-regions, each having a certain characteristic contact area with the top and bottom plates. As the sample radius R increases, the number N of sub-regions scales as the total contact area, which is proportional to R^2 , and consequently $\sigma \sim 1/\sqrt{N} \sim 1/R$.

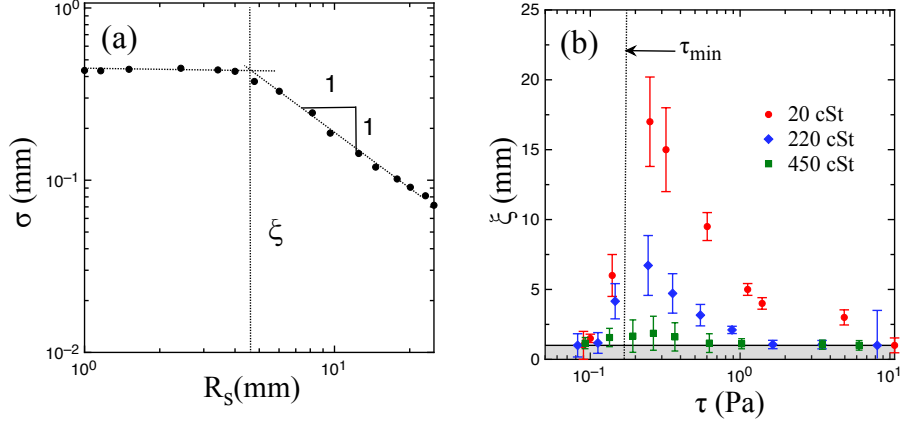


FIG. 5. **Spatial correlations.** (a) Standard deviation σ is plotted against sample radius R_s at $\dot{\gamma} = 0.32 \text{ s}^{-1}$. The transition point from constant to $\sigma \sim 1/R_s$ decay indicates the value of ξ . (b) The plot of ξ vs. $\bar{\tau}$ at $\eta_0 = 20, 220$ and 450 cSt . The dashed line is the onset stress of the shear thickening (τ_{min}). The grey region labels the lower limit of our sample size.

On the other hand, when $R \ll \xi$, the stress across entire sample is spatially correlated such that $\rho(\tau)$ and σ are independent of R_s . Figure 5(a) provides an example to extract the value of ξ . For $\eta_0 = 20 \text{ cSt}$, σ is plotted against R_s for $\dot{\gamma} = 0.32 \text{ s}^{-1}$. It is clear that σ remains constant at small radius and decreases with R_s at large radius. From the plot, we can clearly define a transition point as the correlation length scale $\xi \approx 4.3 \text{ mm}$.

Figure 5(b) plots the lateral correlation length scale, ξ , against the mean value of τ at a given shear rate for different solvent viscosities. For $\eta_0 = 20 \text{ cSt}$ (solid red points), ξ gradually increases with τ when $\tau < \tau_{min}$. Beyond the shear thickening onset τ_{min} , ξ increases dramatically. Here the precision of our standard deviation measurements is not sufficient to tell whether ξ is possibly divergent near τ_{min} . Nevertheless, the sudden increase in ξ in approaching shear thickening regime signals the formation of a network of frictional contacts spanning the measuring gap, consistent with our expectation regarding the mechanisms driving DST. However, as the shear rate further increases into the shear thickening regime, ξ decreases with applied shear stress, as already implied quantitatively in the plots of stress distributions $\rho(\tau)$. As shown in Figure 3(b), the transition from Gamma to Gaussian distributions is a signature of an averaging effect as we ramp up the shear rate. The result suggests a increasing number of independent stress-carrying sub-regions is formed as shear thickening strengthens. A similar trend of ξ is also observed for higher

solvent viscosity. For $\eta_0 = 220$ and 450 cSt (solid blue and green points), although the values of ξ are reduced significantly compared to $\eta_0 = 20$ cSt, the plot shows a quantitatively similar dependence on τ . The values of ξ increase with τ as $\tau < \tau_{min}$, then decrease with τ beyond τ_{min} , and hence peak near the shear thickening onset.

Similar results have been observed in previous works as well. For example, Lootens²⁹ observed a crossover from asymmetric to Gaussian distributions for stress fluctuations of dense colloidal suspensions near the jamming point. In fact, if we interpret strong shear thickening and in particular DST as intermittent jamming behavior, where frictional force chain networks continually form, break up and reconfigure, we would require strong correlations only in the vertical direction that connects the shearing plates. Only for the ultimate limit of a solid-like, shear jammed state might a more isotropic, system-spanning network be expected⁴². Our results thus suggest that shear-induced force networks in DST regime may not be isotropic. We expect further experiments to clarify the issue.

IV. CONCLUSIONS

We show experimentally that viscous interactions in dense granular suspensions can greatly weaken the shear thickening strength and decrease stress fluctuations. First, by comparing steady state rheology measurements for different viscosities η_0 to the Wyart-Cates model, we demonstrate that the frictional jamming point ϕ_j^μ increases with solvent viscosity. The result is equivalent to decreasing thickening strength by lowering the interparticle friction. Second, by systematically measuring stress fluctuations in the shear thickening regime for different η_0 , we quantify how viscous interactions reduce force correlations among particles and weaken the formation of a network of frictional contact forces.

Both results indicate that the solvent viscosity decreases frictional contacts in suspensions. This is likely due to a significant increase of the molecular weight of the polymers as we increase η_0 . For instance, as the viscosity of silicone oil increases by 50 times, the molecular weight can increase orders of magnitude correspondingly. Such long polymer chains can easily be entangled and form a robust lubrication layer as particles are sheared against each other. Our results demonstrate the competition between frictional and viscous interactions in dense suspensions, and they introduce a new approach to control this competition and thereby tune strength of shear thickening.

V. ACKNOWLEDGMENTS

We thank Ivo R. Peters and Carlos S. Orellana for many useful discussions. This work was supported by the the US Army Research Office through Grant No. W911NF-16-1-0078 and the Chicago MRSEC through NSF Grant No. DMR-1420709. A.S. acknowledges support from the Center for Hierarchical Materials Design (CHiMaD).

VI. REFERENCES

REFERENCES

- ¹P. Coussot, *Mudflow rheology and dynamics* (Routledge, 2017).
- ²J. Benbow and J. Bridgwater, “Paste flow and extrusion,” (1993).
- ³J. Mewis and N. J. Wagner, *Colloidal Suspension Rheology* (Cambridge University Press, 2011).
- ⁴E. Brown and H. M. Jaeger, “Shear thickening in concentrated suspensions: phenomenology, mechanisms and relations to jamming.” *Reports on progress in physics* **77**, 046602 (2014).
- ⁵M. M. Denn, J. F. Morris, and D. Bonn, “Shear thickening in concentrated suspensions of smooth spheres in newtonian suspending fluids,” *Soft Matter* **14**, 170–184 (2018).
- ⁶R. Mari, R. Seto, J. F. Morris, and M. M. Denn, “Discontinuous shear thickening in Brownian suspensions by dynamic simulation,” *Proceedings of the National Academy of Sciences* **112**, 15326–15330 (2015).
- ⁷R. Seto, R. Mari, J. F. Morris, and M. M. Denn, “Discontinuous Shear Thickening of Frictional Hard-Sphere Suspensions,” *Physical Review Letters* **111**, 218301 (2013).
- ⁸E. Brown and H. M. Jaeger, “The role of dilation and confining stresses in shear thickening of dense suspensions,” *Journal of Rheology* **56**, 875 (2012).
- ⁹M. Wyart and M. E. Cates, “Discontinuous Shear Thickening without Inertia in Dense Non-Brownian Suspensions,” *Physical Review Letters* **112**, 098302 (2014).
- ¹⁰A. Fall, N. Huang, F. Bertrand, G. Ovarlez, and D. Bonn, “Shear Thickening of Cornstarch Suspensions as a Reentrant Jamming Transition,” *Physical Review Letters* **100**, 018301 (2008).

- ¹¹E. Brown and H. Jaeger, “Dynamic Jamming Point for Shear Thickening Suspensions,” *Physical Review Letters* **103**, 086001 (2009).
- ¹²J. J. Stickel and R. L. Powell, “Fluid Mechanics and Rheology of Dense Suspensions,” *Annual Review of Fluid Mechanics* **37**, 129–149 (2005).
- ¹³M. Maiti and C. Heussinger, “Rheology near jamming: The influence of lubrication forces,” *Physical Review E* **89**, 052308 (2014).
- ¹⁴J. Bender and N. Wagner, “Reversible shear thickening in monodisperse and bidisperse colloidal dispersions,” *Journal of Rheology* **40**(5), 899–916 (1996).
- ¹⁵X. Cheng, J. H. McCoy, J. N. Israelachvili, and I. Cohen, “Imaging the Microscopic Structure of Shear Thinning and Thickening Colloidal Suspensions,” *Science* **333**, 1276–1279 (2011).
- ¹⁶Q. Xu, S. Majumdar, E. Brown, and H. M. Jaeger, “Shear thickening in highly viscous granular suspensions,” *Europhysics Letters* **107**, 68004 (2014).
- ¹⁷N. Y. C. Lin, B. M. Guy, M. Hermes, C. Ness, J. Sun, W. C. K. Poon, and I. Cohen, “Hydrodynamic and Contact Contributions to Continuous Shear Thickening in Colloidal Suspensions,” *Physical Review Letters* **115**, 1–5 (2015).
- ¹⁸N. Fernandez, R. Mani, D. Rinaldi, D. Kadau, M. Mosquet, H. Lombois-Burger, J. Cayer-Barrioz, H. J. Herrmann, N. D. Spencer, and L. Isa, “Microscopic mechanism for shear thickening of non-Brownian suspensions,” *Phys. Rev. Lett.* **111**, 108301 (2013).
- ¹⁹R. Mari, R. Seto, J. F. Morris, and M. M. Denn, “Shear thickening, frictionless and frictional rheologies in non-Brownian suspensions,” *J. Rheol.* **58**, 1693–1724 (2014).
- ²⁰B. M. Guy, M. Hermes, and W. C. K. Poon, “Towards a unified description of the rheology of hard-particle suspensions,” *Phys. Rev. Lett.* **115**, 088304 (2015).
- ²¹C. Ness and J. Sun, “Shear thickening regimes of dense non-Brownian suspensions,” *Soft Matter* **12**, 914–924 (2016).
- ²²C. Clavaud, A. Bérut, B. Metzger, and Y. Forterre, “Revealing the frictional transition in shear-thickening suspensions,” *Proc. Natl. Acad. Sci. U.S.A.* , 5147–5152 (2017).
- ²³J. Comtet, G. Chatté, A. Niguès, L. Bocquet, A. Siria, and A. Colin, “Pairwise frictional profile between particles determines discontinuous shear thickening transition in non-colloidal suspensions.” *Nat. Comm.* **8**, 15633 (2017).
- ²⁴D. Lootens, H. van Damme, Y. Hémar, and P. Hébraud, “Dilatant Flow of Concentrated Suspensions of Rough Particles,” *Physical Review Letters* **95**, 268302 (2005).

- ²⁵C.-P. Hsu, S. N. Ramakrishna, M. Zanini, N. D. Spencer, and L. Isa, “Roughness-dependent tribology effects on discontinuous shear thickening,” *Proc. Nat. Acad. Sci.* (2018).
- ²⁶N. M. James, E. Han, R. A. L. de la Cruz, J. Jureller, and H. M. Jaeger, “Interparticle hydrogen bonding can elicit shear jamming in dense suspensions,” *Nature materials* **17**, 965 (2018).
- ²⁷E. Brown, N. A. Forman, C. S. Orellana, Z. Hanjun, B. W. Maynor, D. E. Betts, J. M. DeSimone, and H. M. Jaeger, “Generality of shear thickening in dense suspensions,” *Nat. Mater.* **9**, 220–224 (2010).
- ²⁸A. Singh, S. Pednekar, J. Chun, M. M. Denn, and J. F. Morris, “From yielding to shear jamming in a cohesive frictional suspension,” *Physical review letters* **122**, 098004 (2019).
- ²⁹D. Lootens, H. Van Damme, and P. Hébraud, “Giant Stress Fluctuations at the Jamming Transition,” *Physical Review Letters* **90**, 178301 (2003).
- ³⁰J. Dasan, T. Ramamohan, A. Singh, and P. Nott, “Stress fluctuations in sheared Stokesian suspensions,” *Physical Review E* **66**, 021409 (2002).
- ³¹B. Miller, C. O’Hern, and R. P. Behringer, “Stress fluctuations in continuously sheared dense granular materials.” *Physical Review Letters* **77**, 3110–3113 (1996).
- ³²D. Howell, R. P. Behringer, and C. Veje, “Stress fluctuations in a 2D granular Couette experiment: a continuous transition,” *Physical Review Letters* **82**, 5241–5244.
- ³³D. Blair, N. Mueggenburg, A. Marshall, H. Jaeger, and S. Nagel, “Force distributions in three-dimensional granular assemblies: Effects of packing order and interparticle friction,” *Physical Review E* **63**, 041304 (2001).
- ³⁴E. I. Corwin, H. M. Jaeger, and S. R. Nagel, “Structural signature of jamming in granular media.” *Nature* **435**, 1075–8 (2005).
- ³⁵E. I. Corwin, E. T. Hoke, H. M. Jaeger, and S. R. Nagel, “Temporal force fluctuations measured by tracking individual particles in granular materials under shear,” *Physical Review E* **77**, 061308 (2008).
- ³⁶A. Singh, V. Magnanimo, K. Saitoh, and S. Luding, “Effect of cohesion on shear banding in quasistatic granular materials,” *Physical Review E* **90**, 022202 (2014).
- ³⁷A. Singh, R. Mari, M. M. Denn, and J. F. Morris, “A constitutive model for simple shear of dense frictional suspensions,” *J. Rheol.* **62**, 457–468 (2018).

- ³⁸J. R. Royer, D. L. Blair, and S. D. Hudson, “Rheological signature of frictional interactions in shear thickening suspensions,” *Phys. Rev. Lett.* **116**, 188301 (2016).
- ³⁹W. H. Boersma, J. Laven, and H. N. Stein, “Shear thickening (dilatancy) in concentrated dispersions,” *AIChE J.* **36**, 321–332 (1990).
- ⁴⁰V. Rathee, D. L. Blair, and J. S. Urbach, “Localized stress fluctuations drive shear thickening in dense suspensions,” *Proceedings of the National Academy of Sciences* **114**, 8740–8745 (2017).
- ⁴¹S. Coppersmith, C. Liu, S. Majumdar, O. Narayan, and T. Witten, “Model for force fluctuations in bead packs.” *Physical review. E* **53**, 4673–4685 (1996).
- ⁴²D. Bi, J. Zhang, B. Chakraborty, and R. P. Behringer, “Jamming by shear,” *Nature* **480**, 355–358 (2011).